Trans. Phenom. Nano Micro Scales, 5(2): 111-129, Summer and Autumn 2017
DOI: 10.7508/tpnms.2017.02.005

ORIGINAL RESEARCH PAPER

Lattice Boltzmann method for MHD natural convection of CuO/water nanofluid in a wavy-walled cavity with sinusoidal temperature distribution

Alireza Shahriari*

Department of Mechanical Engineering, University of Zabol, Zabol, Iran

Received 15 November 2016; revised 11 March 2016; accepted 12 March 2016; available online 10 June 2017

ABSTRACT: In this paper, natural convection heat transfer of CuO-water Nanofluid within a wavy-walled cavity and subjected to a uniform magnetic field is examined by adopting the lattice Boltzmann model. The left wavy wall is heated sinusoidal, while the right flat wall is maintained at the constant temperature of Tc. The top and the bottom horizontal walls are smooth and insulated against heat and mass. The influence of pertinent parameters such as solid volume fraction of nanoparticles (φ), Rayleigh number (Ra), Hartmann number (Ha) and phase deviation of sinusoidal boundary condition (Φ) are investigated on flow and heat transfer fields. Results show that the heat transfer decreases with the increase of the Hartmann number, but it increases by the increment of Rayleigh number and nanoparticle volume fraction. The magnetic field augments the effect produced by the presence of nanoparticles at Ra = 10^4 and 10^5 in contrast with Ra = 10^3. Moreover, the greatest effects of nanoparticles are observed for different values of the phase deviation with an increase in Rayleigh number. This study can, provide useful insight for enhancing the MHD natural convection heat transfer performance within wavy-walled cavity and sinusoidal temperature distribution.

KEYWORDS: *Lattice Boltzmann method; Magnetic field; Nanofluid; Sinusoidal temperature distribution; Wavy-walled cavity*

INTRODUCTION

Laminar natural convection heat transfer is an important phenomenon in engineering and industry due to its frequently occurrence in various engineering applications such as furnaces, heat exchangers, room ventilation, electric machinery, solar technology, MEMS devices, etc. [1-3].

The inherently low thermal conductivity of common fluids used in natural convection such as water, different kinds of oils and ethylene glycol, is considered as the main barrier in increasing heat transfer rate beyond a certain limit. As a solution to this problem, wavy geometries and/or using metal nanoparticles in fluid of heat transfer have been proposed by some authors. As a pioneering work, Choi et al. add nanoparticles (with the size of less than 100 nm) to the base fluid to enhance their thermal conductivity that they called it nanofluid [4]. A nanofluid has unique physical and chemical properties such as dramatic reductions in pumping power, high thermal conductivity and high stability with low sedimentation compared to millimeter or micrometer sized particles and no clogging in micro-channels. Nanofluids have been a subject of considerable amount of research with multifarious methods in recent years due to the increasing importance of them. In an analytical approach conducted by Kim et al. [5], instability of Rayleigh-Bénard natural convection of nanofluids was studied. Their result showed an enhancement in convective heat transfer coefficient of nanofluid due to the presence of nanoparticles.

*Corresponding Author Email: *areza.shahriari@uoz.ac.ir*
Tel.: 09155426651; Note. This manuscript was submitted on November 15, 2016; approved on March 11, 2016; published online June 10, 2017.

Putra et al. [6] carried out an experimental study on the natural convection heat transfer characteristics within a horizontal cylinder filled with Al_2O_3-water and CuO–water nanofluids. Their investigation revealed that natural convection heat transfer decreases by increasing the volume fraction of nanoparticles. The numerical analysis of steady laminar natural convection of nanofluids inside two-dimensional closed enclosures has been studied by many authors. A numerical investigation of buoyancy-driven heat transfer enhancement was done by Khanafer et al. [7] in a differentially heated square cavity utilizing Cu–water nanofluid for the range of Grashof numbers between 10^3 and 10^5. They concluded that heat transfer across the enclosure increases with an increase in the percentage of the suspended nanoparticles at all range of Grashof numbers. From the other side, problem of natural convection exposed to a magnetic field is of paramount importance in engineering applications because of its ability to control the fluid flow with no physical contact. The magnetohydrodynamic (MHD) forces are also active for an electrically conducting fluid flow in presence of a magnetic field and the Lorentz force interacts with the buoyancy force in governing the flow and temperature fields. The importance tasks of hydro- magnetic flow and heat transfer in technological and industrial applications such as geothermal energy extractions, polymer industry and metallurgy, crystal growth in liquids, metal casting, fusion reactors has resulted in extensive research in the open literature so far. [8-12].

Various investigations on natural convection of nanofluid

Nomenclature

A	Dimensionless amplitude	α	Thermal diffusivity ($m^2\ s^{-1}$)
B	Magnetic field	β	Thermal expansion coefficient (K^{-1})
C_p	Heat capacity ($J\ kg^{-1}\ K^{-1}$)	φ	Nanoparticles volume fraction
f_i	Particle distribution function	μ	Dynamic viscosity ($kg\ m^{-1}\ s^{-1}$)
g_i	Energy distribution functions	ρ	Density ($kg\ m^{-3}$)
g	Gravity ($m\ s^{-2}$)	σ	electrical conductivity
H	Height of cavity (m)	$\theta = \frac{T-T_C}{T_H-T_C}$	Non-dimensional temperature
Ha	Hartmann number	τ	Relaxation time
k	Thermal conductivity($W\ m^{-1}\ K^{-1}$)		**Subscripts**
W	Length of cavity (m)	eq	equilibrium state
n	Number of roughness elements	f	Fluid
Nu_m	mean Nusselt number	nf	nanofluid
Pr=ϑ/α	Prandtl number	p	nanoparticle
$Ra = \frac{g_y \beta H^3 \Delta T}{\vartheta \alpha}$	Rayleigh number	ϑ	Velocity
T	Temperature (K)	T	Thermal

in the presence of magnetic field have been performed by researchers with applying different numerical methods.

In two recent decades, lattice Boltzmann method (LBM) has been used as an alternative method to Navier-Stokes equations for fluid flow simulation, due to its advantages such as simplicity of programming, easy of parallel coding because of its local nature, ease of simulation of complex geometries and complex flows such as multiphase and multicomponent flows [13-15]. Curved boundary treatment is a straightforward procedure in LBM. Fillipova and Hanel [16] used boundary fitting method to simulate curved boundaries in LBM while Mei et al. [17] improved its numerical stability later. Guo et al. [18] divided the distribution function for temperature into two parts, equilibrium and nonequilibrium. They proposed the so-called ‘‘extrapolation method’’ which is developed using basic extrapolation scheme.

In general, numerical simulations of MHD natural convection in a nanofluid-filled cavity fall into three main categories: a) cavities with smooth walls and uniform temperature distribution; b) cavities with smooth walls and non-uniform temperature distribution; c) cavities with curve boundaries and uniform temperature distribution. For example, a number of these papers that were published recently can be named.

Ghasemi et al. [19] investigated the effect of magnetic field on natural convection heat transfer performance of nanofluid in a square enclosure by two isothermal flat vertical walls. The results of these researchers indicate that the effect of the enhancement of the solid volume fraction on the heat transfer performance is significantly depended on both values of Rayleigh number and Hartmann number. Moreover, they indicated that the heat transfer rate increases with a growth of the Rayleigh number, but it decreases with a growth of the Hartmann number. Kefayati [20] utilized the LBM to simulate the magnetic field effects on natural convection heat transfer in an open cavity subjugated to Al_2O_3-water nanofluid. He observed that average Nusselt number declines with a rise of Hartmann number for different values of Rayleigh numbers and solid volume fractions. Furthermore, it emerged the effect of nanoparticles increases regularly with increasing Hartmann number in high Rayleigh number.

Kefayati [21] investigated natural convection MHD in a nanofluid-filled cavity with sinusoidal heated right wall using lattice Boltzmann method. It was observed that the heat transfer declines with increasing of Hartmann number and marginal reduction was acquired at Ra = 10^3 compared with other Rayleigh numbers. Also, in the absence of the magnetic field, the most effects of nanoparticles was found as phase deviation equals to the Φ = 3π/4, 0 and π/2 for Ra = 10^3, 10^4 and 10^5 respectively. Mliki et al. [22] scrutinized augmentation of natural convective heat transfer in a nanofluid-filled cavity with a linearly heated wall under the influence of magnetic field and uniform heat generation or absorption using LBM. They reported that without the heat generation or absorption source, the magnetic field controls the nanoparticles influence for increment or decrement of the heat transfer performance. Moreover, the results revealed that uniformly temperature distribution on left wall exhibits larger enhancement of heat transfer as compared to linearly and sinusoidal temperature distributions.

Sheikholeslami et al. [23] employed a D2Q9 lattice model in order to simulate the natural convection heat transfer utilizing Al_2O_3-water nanofluids in a square cavity with curve boundaries using KKL correlation. They proved that the Nusselt number has a direct relationship with nanoparticle volume fraction and Rayleigh number, but it has a reverse relationship with the Hartmann number. Furthermore, their results indicated that at Ra=10^4, there is a critical Hartmann number at which the enhancement of heat transfer between the nanofluid and the base fluid ratio reaches its maximum. Sheremet et al. [24] investigated the unsteady natural convection in a wavy porous enclosure

filled with a nanofluid under the influence of magnetic field. They found that the convective flow and heat transfer heat rate attenuates with increasing Hartmann number and a double-core convective cell was formed for high values of Ha.

In addition, they reported that increasing the heating of the wavy troughs due to increasing the undulation number leads to a decrease in the average Nusselt number.

Despite the numerous studies of the natural convection in cavities with smooth walls, cavities with non-uniform temperature distribution on smooth wall and cavities with curve boundaries, there are fewer studies on the natural convection in cavities with non-uniform distribution on curve boundaries.

This type of problem is found in the majority practical problem. For example, in the solar collector, there is a network of tubes plated against the absorber, which the variation in temperature along it were simulated by a sinusoidal law. This kind of heating is also observed in the glass technology and in crop drying process such as corn and rice [25].

Sabeur-Bendehina et al. [25] studied laminar natural convection heat transfer in an undulated inclined rectangular cavity with non-uniform boundary conditions. They found that the distribution of the temperature leads to wavy tendency of the local Nusselt number not to the geometry of the hot wavy wall.

Recently, Shahriari [26] has done a numerical simulation of free convection heat transfer of nanofluid in a wavy-wall cavity with sinusoidal temperature distribution, using lattice Boltzmann method. He reported that for a fixed Rayleigh number, the heat transfer performance depends on tuning the wavy-surface geometry parameters.

The literature mentioned above shows that the cases of wavy-wall enclosed cavity and non-uniform heated cavity in the presence of magnetic field are studied separately. However, no published work was found in which, MHD natural convection of a nanofluid in a wavy-walled cavity with non-uniform temperature distribution is studied. Therefore, the present paper is devoted to simulate such flow configuration with LBM. In the present study, lattice Boltzmann method is applied to simulate MHD natural convection heat transfer of CuO-water nanofluid in a wavy-walled cavity with sinusoidal temperature distribution.

PROBLEM STATEMENT AND MATHEMATICAL MODELING

Problem statement

A schematic representation of a wavy-walled cavity is shown in Figure 1 which is filled with CuO-water nanofluid. As it is observed in this figure, the left wavy wall is heated sinusoidal, while the right flat wall is maintained at a temperature Tc.

The horizontal upper and lower walls are assumed to be insulated. A uniform magnetic field with constant magnitudes is applied horizontally normal to the side walls. Nanofluid within the cavity is initially at rest. Then, fluid motion is induced by buoyancy force driven by temperature difference between left and right walls.

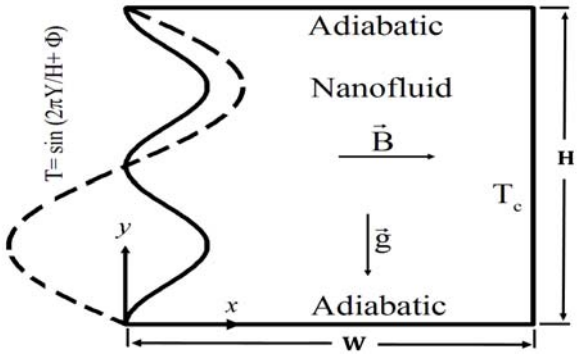

Fig.1. Schematic representation of the system under consideration

It is considered that the left wavy wall and the right flat wall of the cavity are presented by the relations:

$$x = A\left(1 - cos\left(\frac{2\pi nY}{H}\right)\right) \quad \text{for left wall}$$
$$x = \frac{W}{H} \quad \text{for right wall} \tag{1}$$

where A and n are dimensionless amplitude of the wavy wall and number of undulation, respectively.

Thermo-physical properties of nanofluid

In the present study, the flow of electrically, conducting nanofluid which consists of water and CuO nanoparticles is subjected to the assumptions of incompressible, single-phase, no-chemical reaction, no-slippage between base fluid and solid nanoparticles, negligible thermal radiation and viscous dissipation due to its small effects. Also, the flow is supposed to be laminar, steady and incompressible with thermo-physical properties of base fluid and nanoparticles tabulated in Table 1.

Table 1. Thermo-physical properties of base fluid and nanoparticles.

Property	Nanoparticles (CuO)	Base fluid (water)
$\rho(kg/m^3)$	6500	997.1
$C_P(J/kgK)$	540	4179
$k(W/mK)$	18	0.613
$\beta \times 10^5(1/K)$	0.85	21

The value of Prandtl number is selected as 6.2 for temperature of 300 K.

The variations of thermo-physical properties of the nanofluid are negligible with respect the temperature, except in Boussinesq approximation. The induced magnetic field produced by the motion of an electrically conducting fluid is assumed to be negligible by comparison with the applied external magnetic field.

It is considered that the nanofluid is a single phase fluid, thus the addition of nanoparticles to the base fluid has significant effects on thermo-physical properties of the nanofluid.

The effective density ρ_{nf}, the specific heat $(c_p)_{nf}$, thermal expansion coefficient β_{nf} and electrical conductivity σ_{nf} of the nanofluid are expressed as [27]:

$$\rho_{nf} = (1-\varphi)\rho_f + \varphi\rho_p \tag{2}$$

$$(c_p)_{nf} = \left[\frac{1}{1+\frac{(1-\varphi)\rho_f}{\varphi\rho_p}\frac{(c_p)_p}{(c_p)_f}+\frac{1}{1+\frac{\varphi\rho_p}{(1-\varphi)\rho_f}}}\right](c_p)_f \tag{3}$$

$$\beta_{nf} = \left[\frac{1}{1+\frac{(1-\varphi)\rho_f}{\varphi\rho_p}\frac{\beta_p}{\beta_f}+\frac{1}{1+\frac{\varphi\rho_p}{(1-\varphi)\rho_f}}}\right]\beta_f \tag{4}$$

$$\sigma_{nf} = \left[1+\frac{3(\frac{\sigma_s}{\sigma_f}-1)\varphi}{\left(\frac{\sigma_s}{\sigma_f}+2\right)-(\frac{\sigma_s}{\sigma_f}-1)\varphi}\right]\sigma_f \tag{5}$$

here, φ is the solid volume fraction of nanoparticles and the subscripts nf, f and p denote the nanofluid, base fluid and solid nanoparticles, respectively.

Effective dynamic viscosity, μ_{nf} and the effective thermal conductivity, k_{nf} of the nanofluid which are obtained from Brinkman [28], and Hamilton and Crosser [29] models respectively, are expressed as:

$$\mu_{nf} = \frac{\mu_f}{(1-\varphi)^{2.5}} \tag{6}$$

$$k_{nf} = \frac{k_{p+}(n-1)k_f - (k_f - k_p)(n-1)\varphi}{k_{p+}(n-1)k_f + (k_f - k_p)\varphi}\,k_f \tag{7}$$

Finally, the thermal diffusivity of the nanofluid is defined as:

$$\alpha_{nf} = \frac{k_{nf}}{(\rho C_p)_{nf}} \tag{8}$$

Lattice Boltzmann method

In the present work, a standard two-dimensional nine-velocity (D_2Q_9) LBM with single relaxation time collision operator is employed for both flow and temperature (fig. 2).

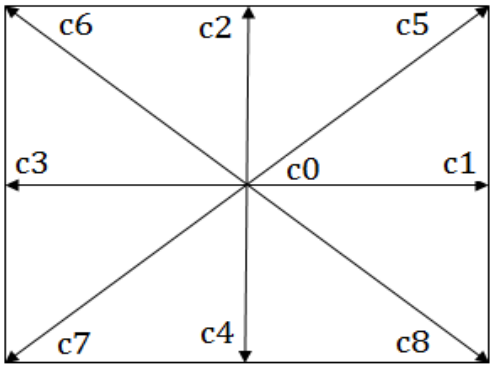

Fig. 2. Discrete velocity vectors for the D2Q9 model

Lattice Boltzmann equation for the evolution of velocity field in discretized form is expressed as [30, 31]:

$$f_i(x + c_i\Delta t.\, t + \Delta t) = f_i(x.t) - \frac{\Delta t}{\tau_\vartheta}[f_i(x.t) - f_i^{eq}(x.t)] \tag{9}$$

in which, f_i is the particle distribution function along the i^{th} direction. In D_2Q_9 lattice model, discrete velocity vectors, c_i, are given as:

$$\begin{aligned} &c_i = 0, i = 0 \\ &c_i = c(\cos\theta_i, \sin\theta_i);\ \theta_i = (i-1)\tfrac{\pi}{2},\ i = 1,2,3,4 \\ &c_i = c\sqrt{2}(\cos\theta_i, \sin\theta_i);\ \theta_i = (i-5)\tfrac{\pi}{2} + \tfrac{\pi}{4}, \\ &i = 5,6,7,8 \end{aligned} \tag{10}$$

Equilibrium distribution function f_i^{eq} is defined as:

$$f_i^{eq} = \omega_i\rho\left[1 + 3\frac{c_i.u}{C^2} + \frac{9}{2}\frac{(c_i.u)^2}{C^4} - \frac{3}{2}\frac{u^2}{C^2}\right] \tag{11}$$

where ρ and u are the macroscopic fluid density and velocity, respectively, and ω_i are weighting coefficients that are defined as follows:

$$\omega_i = \begin{cases} 4/9 & i = 0 \\ 1/9 & i = 1,2,3,4 \\ 1/36 & i = 5,6,7,8 \end{cases} \tag{12}$$

Kinetic viscosity and relaxation time are related to each other as:

$$\vartheta = {C_s}^2\Delta t(\tau_\vartheta - 0.5) \tag{13}$$

where, C_s is the speed of sound which is equal to $\frac{C}{\sqrt{3}}$.

Macroscopic mass density and velocity can be expressed in terms of particle distribution function as follows:

$$\rho = \sum_{i=0}^{8} f_i \tag{14}$$

$$\rho U = \sum_{i=0}^{8} c_i f_i \tag{15}$$

Numerical implementation of lattice Boltzmann equation (Eq. 8) can be done in two steps, namely collision and streaming:

$$\tilde{f}_i(x, t+\Delta t) = f_i(x,t) - \frac{\Delta t}{\tau_\vartheta}[f_i(x,t) - {f_i}^{eq}(x,t)] \quad \text{Collision} \tag{16}$$

$$f_i(x + c_i\Delta t, t+\Delta t) = \tilde{f}_i(x, t+\Delta t) \quad \text{Streaming} \tag{17}$$

The $\tilde{f}$ in the above equations refer to post-collision state of the particle distribution functions.

The buoyancy force in the present natural convection heat transfer problem is treated as an external force term, which is added to the basic form of lattice Boltzmann equation as following:

$$f_i(x + c_i\Delta t, t+\Delta t) = f_i(x,t) - \frac{\Delta t}{\tau_\vartheta}[f_i(x,t) - {f_i}^{eq}(x,t)] + \Delta t c_i F_i(x,t) \tag{18}$$

in which, F_i is the external force term in direction of lattice velocity and to incorporate buoyancy forces and magnetic forces in the model, it can be conducted as [32]:

$$\begin{aligned} F &= F_X + F_Y \\ F_x &= 3w_i\rho[D(v\sin(\theta)\cos(\theta) - (u\sin^2(\theta)))] \\ F_y &= \\ &3w_i\rho\big[g_y\beta(T(x,t) - T_\infty) + D(u\sin(\theta)\cos(\theta) - \\ &(v\cos^2(\theta)))\big] \end{aligned} \tag{19}$$

where T_∞, β and θ are reference temperature, thermal expansion coefficient and direction of the magnetic field, respectively, and D is defined as:

$$D = \frac{Ha^2\,\mu}{L^2} \tag{20}$$

The dimensionless parameter Ha is the Hartmann number, which is defined as the ratio of Lorentz force to viscous forces with the following formulas:

$$Ha = LB_0\sqrt{\frac{\sigma}{\mu}} \tag{21}$$

where B_0 and σ are magnetic flux density and electrical conductivity.

Similar equation can be written for temperature distribution function, g. Neglecting viscous dissipation and compressive heating effects, energy distribution function is expressed as:

$$g_i(x + c_i\Delta t, t+\Delta t) = g_i(x,t) - \frac{\Delta t}{\tau_T}[g_i(x,t) - {g_i}^{eq}(x,t)] \tag{22}$$

in which, g_i is temperature distribution function in i^{th} direction and τ_T is the dimensionless relaxation time. Also, equilibrium energy distribution function, g^{eq}, for D_2Q_9 model can be written as [18]:

$$ {g_i}^{eq} = \omega_i T\left[1 + 3\frac{c_i u}{C^2} + \frac{9}{2}\frac{(c_i u)^2}{C^4} - \frac{3}{2}\frac{u^2}{C^2}\right] \tag{23}$$

Temperature is calculated through the following Equation:

$$T = \sum_{i=0}^{8} g_i \tag{24}$$

Here thermal diffusivity is related to relaxation time of temperature distribution function as:

$$\alpha = {C_s}^2\Delta t(\tau_T - 0.5) \tag{25}$$

Boundary conditions

Boundary conditions used in the present study can be expressed in non-dimensional form as:

For the left wall

$$U = V = 0 \qquad \theta = sin(\frac{2\pi Y}{H} + \phi)$$

For the right wall

$$U = V = 0 \qquad \theta = 0 \tag{26}$$

For the top and bottom walls

$$U = V = 0 \qquad \frac{\partial\theta}{\partial y} = 0$$

The no-slip and no-temperature-jump boundary conditions at solid walls were implemented using the models of Mei et al. [17] and Guo et al. [18]. In the curved boundary scheme, distribution functions on the boundary nodes are unknown. Thus, a linear interpolation is used to specify the unknown values of the distribution functions. The linear interpolation consists of two parts: the first part is the post-collision distribution functions at the fluid node near the boundary wall and the second part is fictitious equilibrium distribution functions at the neighboring solid node. The schematic of an orthogonal equidistant lattice

structure near a curved wall boundary separating a solid region from fluid and lattice nodes are shown in Figure 3. In this figure, the black solid circles represent the wall nodes, x_w, the open circles refer to the fluid nodes, x_f and the grey solid circles indicate those in the solid region, x_b.

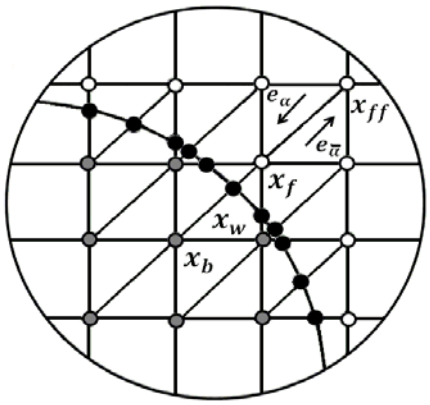

Fig. 3. Curved wall boundary and lattice nodes

Finally, in order to evaluate the heat transfer rate, local Nusselt number and mean Nusselt number on each isothermal wall as well as its normalized value are obtained as:

$$Nu_l = -\frac{k_{nf}}{k_f}\left(\frac{\partial\theta}{\partial n}\right) \tag{27}$$

$$Nu_m = \frac{1}{H}\int_0^1 \sqrt{Nu_l^2}\; dy^* \tag{28}$$

$$Nu^* = \frac{Nu_{m(\varphi)}}{Nu_{m(\varphi=0)}} \tag{29}$$

Validation

As a first step in a computational method, it is required to have results that are not depended on grid resolution. To this end, as is observed in Table 2, five lattice grids are used and mean Nusselt number (Nu_m) for different grid resolutions at Ra = 10^4 is calculated.

Table 2
The mean Nusselt number on hot wavy-wall surface for different grids at Ha = 30, φ = 0.04 and Φ = 0.

Grid size Nx × Ny	Mean Nusselt number (Nu_m)
21 × 21	2.52525
41 × 41	4.62309
81 × 81	4.19835
101 × 101	3.99583
141 × 141	3.95413

It is found, from this table, that a grid independent solution can be obtained for a grid distribution of at least101×101 grid points. Hence, a grid size of 101×101 points is used in all computations to compromise between computational cost and accuracy.

Convergence criterion used in the present study is expressed as:

$$\varepsilon = \frac{\sum_{i=1}^{i=N}\sum_{j=1}^{j=M}|T^{n+1}-T^n|}{\sum_{i=1}^{i=N}\sum_{j=1}^{j=M}|T^n|} < 10^{-7} \tag{30}$$

in which, 'n', 'n+1', ε , N and M represent old time level, new time level, tolerance, number of grid points in x and y-directions, respectively.

To validate the present computational procedure, analysis was done for a system containing pure fluid in a square cavity with Pr = 0.7 and different Rayleigh numbers. Table 3 shows comparison of the present computations with previous published works.

Table 3
Comparison of results with previous works in a square cavity for Pr = 0.7 with different Rayleigh numbers.

	Present	Davis [1]	Tiwari and Das [33]	Lin and Violi [34]
Ra = 10^3				
U_{max}	3.652	3.649	3.642	3.597
y	0.820	0.813	0.804	0.819
V_{max}	3.753	3.697	3.703	3.690
x	0.186	0.178	0.178	0.181
Nu	1.119	1.118	1.087	1.118
Ra = 10^5				
U_{max}	35.45	34.73	34.30	36.70
y	0.863	0.855	0.856	0.858
V_{max}	68.78	68.59	68.77	68.29
x	0.075	0.066	0.059	0.063
Nu	4.480	4.519	4.450	4.511

The parameters considered in this comparison are maximum horizontal velocity on the vertical midplane of the cavity, U_{max} , and the corresponding y-coordinate, the maximum vertical velocity on the horizontal midplane of the cavity, V_{max} , and the corresponding x-coordinate, and the average Nusselt number for cavity. This table shows an excellent agreement between the present results and other benchmark solutions. Figure 4 shows results which confirm the accuracy of the present computations with the experiment ones of Krane and Jessee [35], numerical simulation of Oztop and Abu-Nada [36] and numerical simulation of Khanafer et al. [7] for Ra = 10^5 and Pr = 0.7. The present code has been further validated through published studies in the literature on the cavity with complex wavy surface containing nanofluid [37]. The qualitative comparison of streamlines and isotherms in the

present study with those in Ref. [37] show good correspondence (see fig. 5). Mean Nusselt number on hot wall for different Hartmann numbers in the square cavity is shown in Table 4 with those of other numerical investigations.

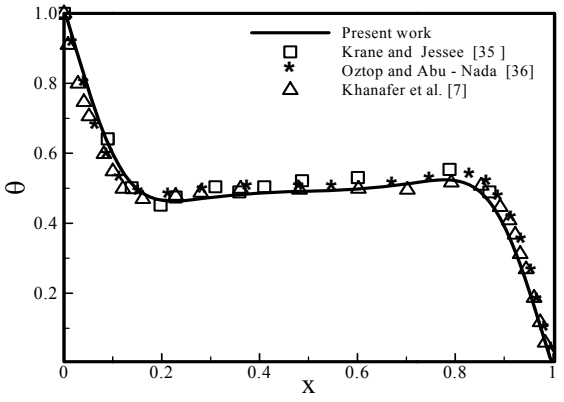

Fig. 4. Comparison of results of temperature distribution at the vertical mid-section along the width of the square cavity with those in the literature ($Ra = 10^5$, $Pr = 0.7$)

Table 4
Comparison of the mean Nusselt numbers on hot wall for different Hartmann numbers in the square cavity.

	Present study	**Ghasemi et al. [19]**	**Kefayati [38]**	**Ahrar and Djavareshkian [39]**
Ha = 0	4.6865	4.738	4.794	4.722
Ha = 15	4.1006	4.143	------	------
Ha = 30	3.1203	3.150	3.224	3.143
Ha = 45	2.3461	2.369	------	------
Ha = 60	1.8311	1.851	1.900	1.865
Ha = 90	1.3145	------	1.356	------

Good correspondence is observed between present computations and previous works. In addition, comparison of streamlines and the isotherms in the square cavity against the study Ghasemi et al. [19] for $Ra = 10^5$ shows good agreement, as is observed in figure 6.

RESULTS AND DISCUSSION

For this part of the analysis, a representative set of graphical results are depicted to show the effects of the various physical parameters on the hydrodynamic and thermal behavior of nanofluid in a wavy-walled cavity with sinusoidal temperature distribution in the presence of a uniform magnetic field.

Rayleigh and Hartmann number

In this section, it is assumed that solid volume fraction of nanoparticles and phase deviation of boundary conditions are set to $\varphi = 0.04$ and $\Phi = 0$, respectively. This phase deviation means that the left wavy wall of the cavity is heated from the bottom half wall and cooled from the top half wall, whereas the right flat wall is maintained at a constant temperature of Tc = 0. Figures 7 and 8 show effect of Hartmann number on streamlines and isotherms contours for three different Rayleigh numbers ($Ra = 10^3$, 10^4 and 10^5) and four percent volume fraction of CuO nanoparticles in the enclosed cavity.

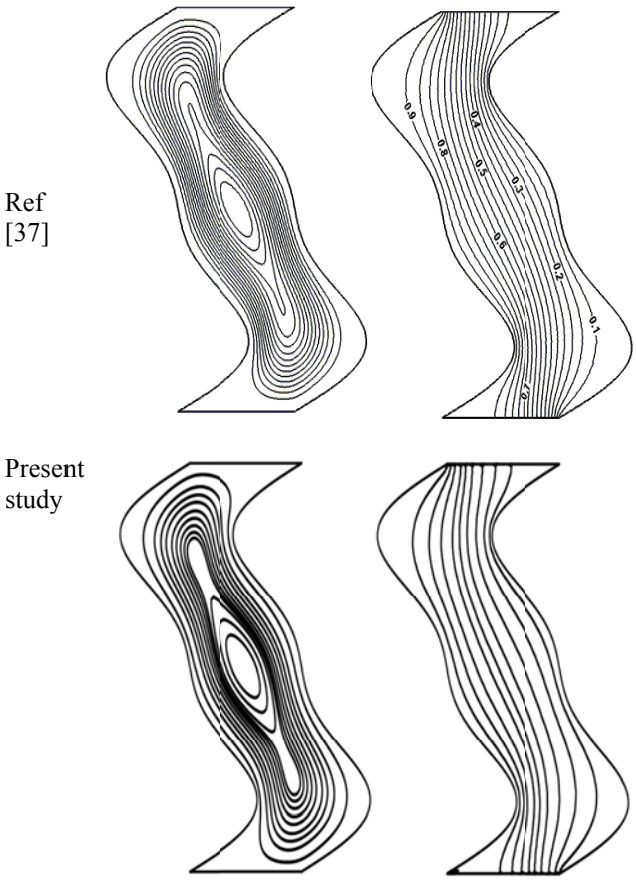

Fig. 5. Comparison of the streamlines (left) and isotherms (right) between numerical results by Cho et al. [37] and the present results

It is clearly depicted from Figure 7 that the streamlines are characterized with the buoyancy-driven flow by two circulation cells for all values of Hartmann and Rayleigh numbers.

These two cells have symmetrical structures with respect to the middle of the vertical wall and they rotate in opposite direction inside the enclosure.

The cell located in the bottom part of the cavity turns in the clockwise direction due to the existence of heat source at this place. Therefore, the heat energy is transported from the lower half to the upper half. In addition, the convection process rises as the Rayleigh number increases whereas convection flow declines as the power of the magnetic field increases.

Figure 8 shows that the isotherms are also influenced due to variations in the Rayleigh and Hartmann numbers. It can be seen that intersection of isotherm line with the wavy wall due to non-uniform temperature distribution causes formation of cells on wavy wall.

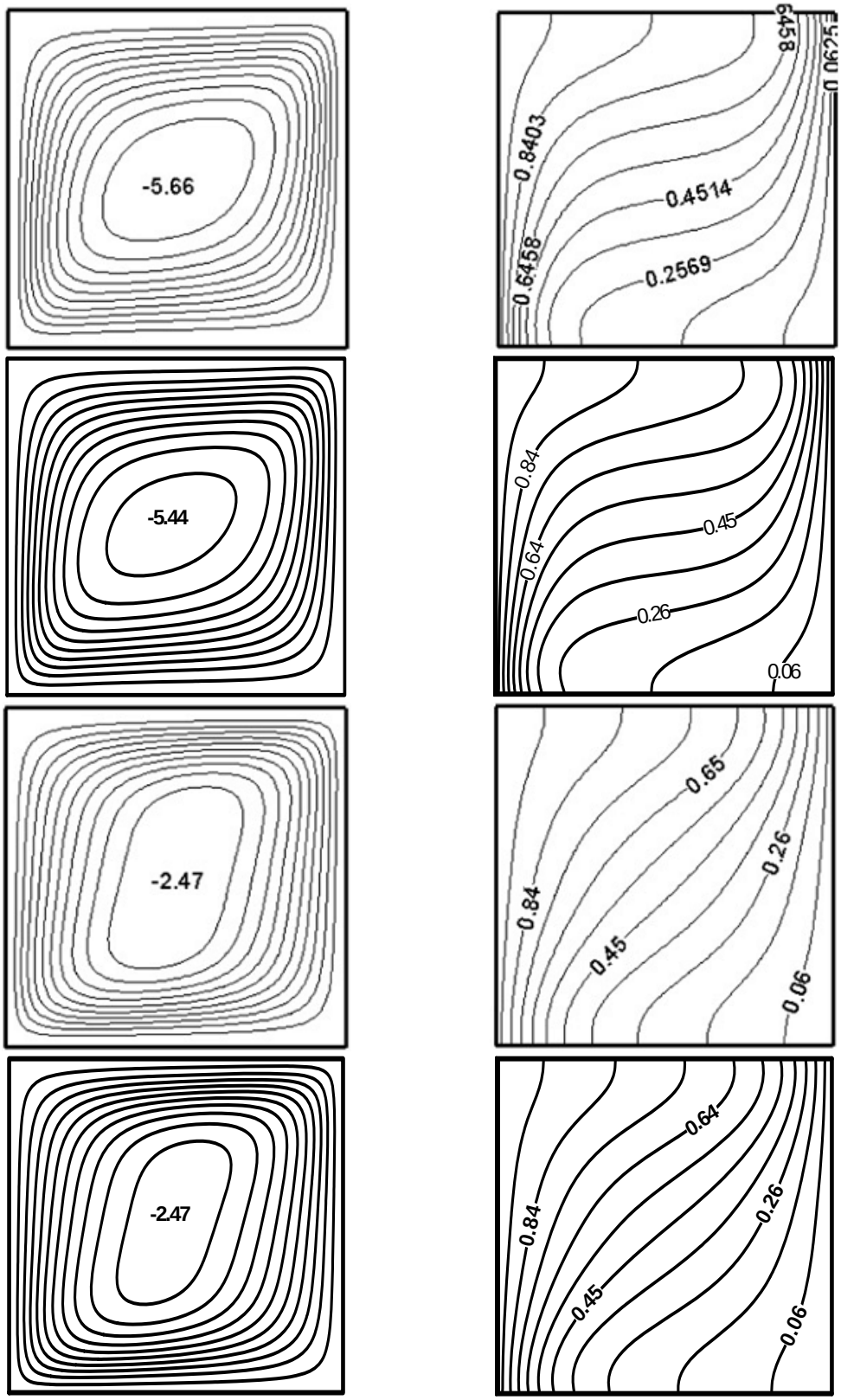

Fig. 6. Comparison of the streamlines (left) and isotherms (right) between numerical results by Ghasemi et al. [19] and the present results at Ra = 10^5

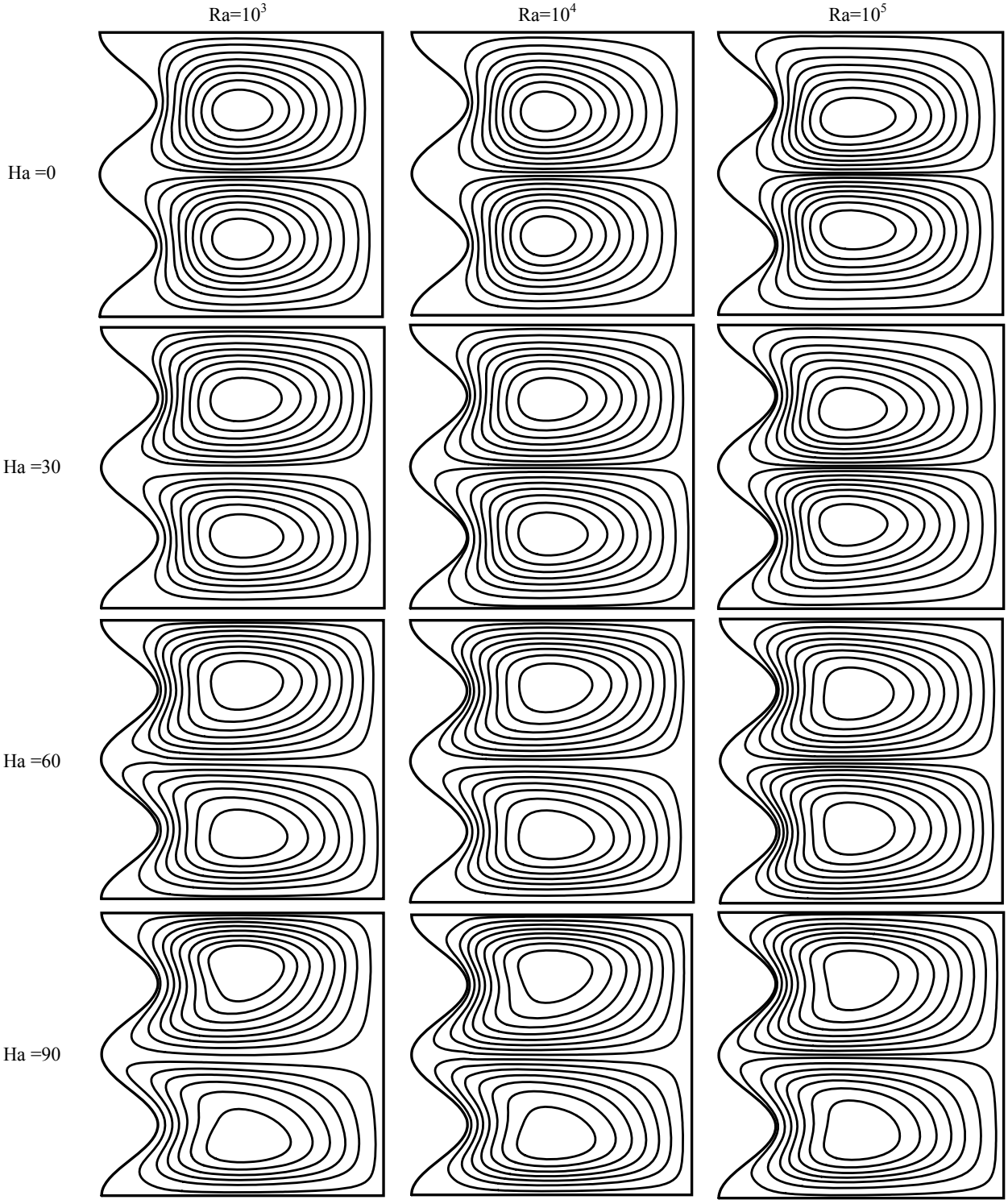

Fig. 7. Comparison of the streamlines contours for different Rayleigh and Hartmann numbers ($\varphi = 0.04$, $\Phi = 0$)

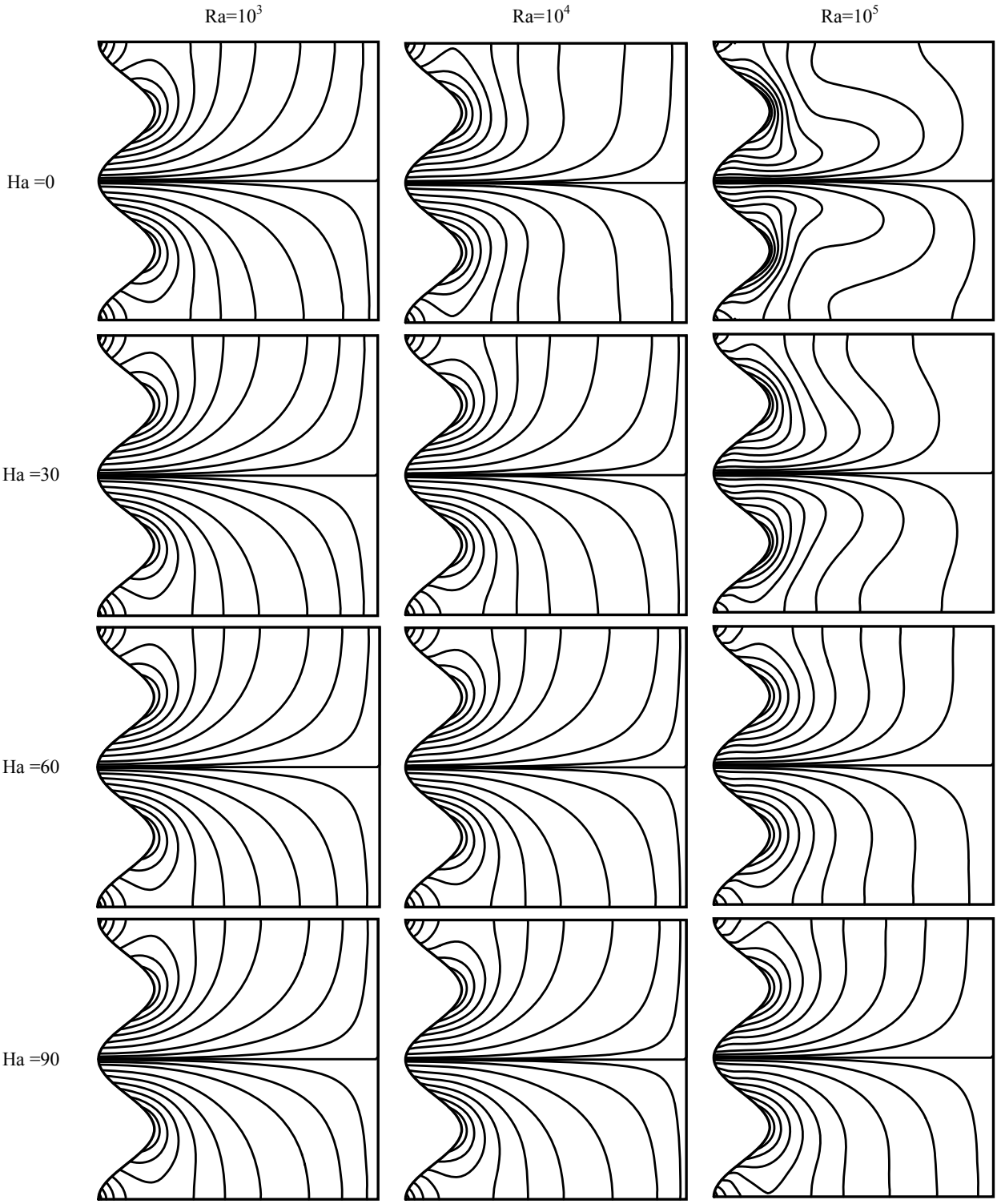

Fig. 8. Comparison of the isotherms contours for different Rayleigh and Hartmann numbers ($\varphi = 0.04$, $\Phi = 0$)

The numbers of these cells depend on separate thermal sections. Moreover, the isotherms are affected in the presence of a magnetic field, especially at high Rayleigh numbers. At Ra = 10^4, as the power of the magnetic field augments, difference between the compared isotherms will more noticeable than Ra = 10^3. By increasing the magnetic force at Ra = 10^5, first of all causes the isotherms become modification, less curved and more parallel to the isothermal right wall. Where isotherms move further from the left wavy wall and leads to the gradient of the temperature to fall on wavy wall.

This shows the heat transfer regime goes from conduction dominant to convection dominant system at higher Hartmann numbers.

Figure 9 depicts variations of maximum absolute stream function with Hartmann number as a function of Rayleigh number at φ = 0.04 and Φ = 0.

This figure demonstrates that increasing of Hartmann number decreases the strength of the circulation structure within the cavity due to augmentation of the braking effect of the magnetic field. In addition, it is obvious that the rate of this decrease is different for various values of Rayleigh numbers. For example, from Ha = 0 to 90 the decreasing rate for the maximum absolute stream function $|\psi_{max}|$, is about 7.8%, 1.6% and 0.2% for Rayleigh numbers of Ra = 10^3, 10^4 and 10^5, respectively. Moreover, this figure explores that effect of Hartmann number is opposite to the behavior registered of Rayleigh number.

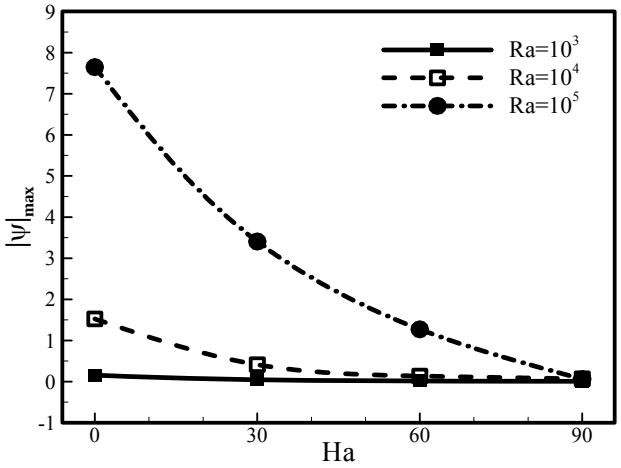

Fig. 9. Variation of the maximum of the stream function with Hartmann number for different Rayleigh number (φ = 0.04, Φ = 0)

Figure 10 illustrates variation of the local Nusselt number along hot wavy-wall surface for two Rayleigh numbers (Ra = 10^3 and Ra = 10^5) at various Hartmann numbers.

The local Nusselt number exposes a similar manner, decreasing with increase in Hartmann number for both values of Rayleigh numbers. It is clearly observed that for Ra = 10^3 the local Nusselt number gets little change on left wavy wall even as the Ha is increased to 90, whereas it declines noticeable at Ra = 10^5. Furthermore, it must be noted that variation of local Nusselt number is marginal with the enhancement of Hartmann number from Ha = 30 to 60 at Ra = 10^5.

Figure (11a) illustrates how the mean Nusselt number varies with Hartmann number at various values of Rayleigh numbers.

Figure (11b) illustrates the effects of the Rayleigh and Hartmann number on dimensionless mean Nusselt number that normalized with respect to mean Nusselt number for the pure hydrodynamic. Firstly, it can be observed from the Figure 11 that mean Nusselt number increases when the Rayleigh number increases from Ra = 10^3 to 10^5.

This is due to increasing Rayleigh number and hence buoyancy force causes the thickness of the thermal boundary layer to reduce.

As a result, more convection effects occur and thus the mean Nusselt number increases. Secondly, it can be seen that the mean Nusselt number declines with the increasing Hartmann number for all cases of Rayleigh numbers except for Ra = 10^3. This is due to Lorentz force that is produced by an applied magnetic field that counteracts to the buoyancy force.

Also, the rate of variation is a function of the Rayleigh number, as shown in Figure (11b).

At Ra = 10^3, the dominating heat transfer mechanism is only due to conduction and the presence of magnetic field does not have a remarkable effect on heat transfer as the Hartmann number increases.

However, the magnetic field has a remarkable effect on Nusselt number by increasing the Rayleigh number. For example, for Ha = 90, the decrement in normalized mean Nusselt number for Ra = 10^4 is about 4% whereas the decrease is around 29% for Ra = 10^5.

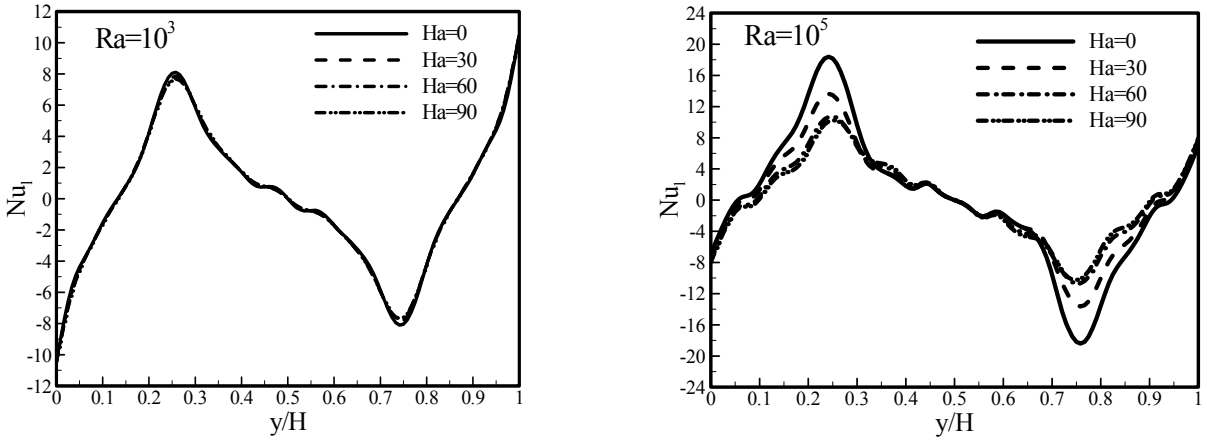

Fig. 10. Variation of local Nusselt number along hot wavy-wall surface for different Hartmann number (φ = 0.04, Φ = 0)

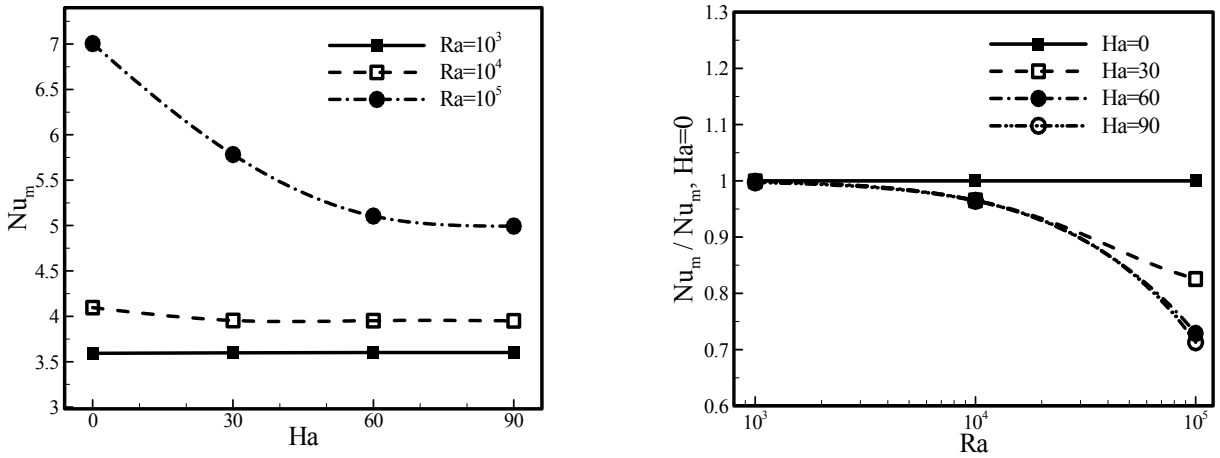

Fig. 11. Variation of mean Nusselt number and normalized mean Nusselt number with Rayleigh and Hartmann numbers (φ = 0.04, Φ = 0)

Nanoparticle volume fraction

For this section of the study, the effect of addition of nanoparticles on flow and heat transfer has been analyzed for different Rayleigh and Hartmann numbers while keeping the phase deviation constant equal to Φ = 0.

Figure 12 shows comparison of streamline and isotherm contours for three different Hartmann numbers, as Ra equals to 10^5. The streamline contours show that the upper and lower vortexes in the cavity become larger in size and stronger in strength as volume fraction increases, if magnetic field is ignored. However, the value of absolute circulation strength ($|\psi|_{max}$) decreases by the addition of nanoparticles in the presence of a magnetic field. As it is observed in this figure, the isotherms have the same pattern to a pure conduction for a strong magnetic field.

from the top half and hence resulted in symmetrical structures for streamlines and isotherms.

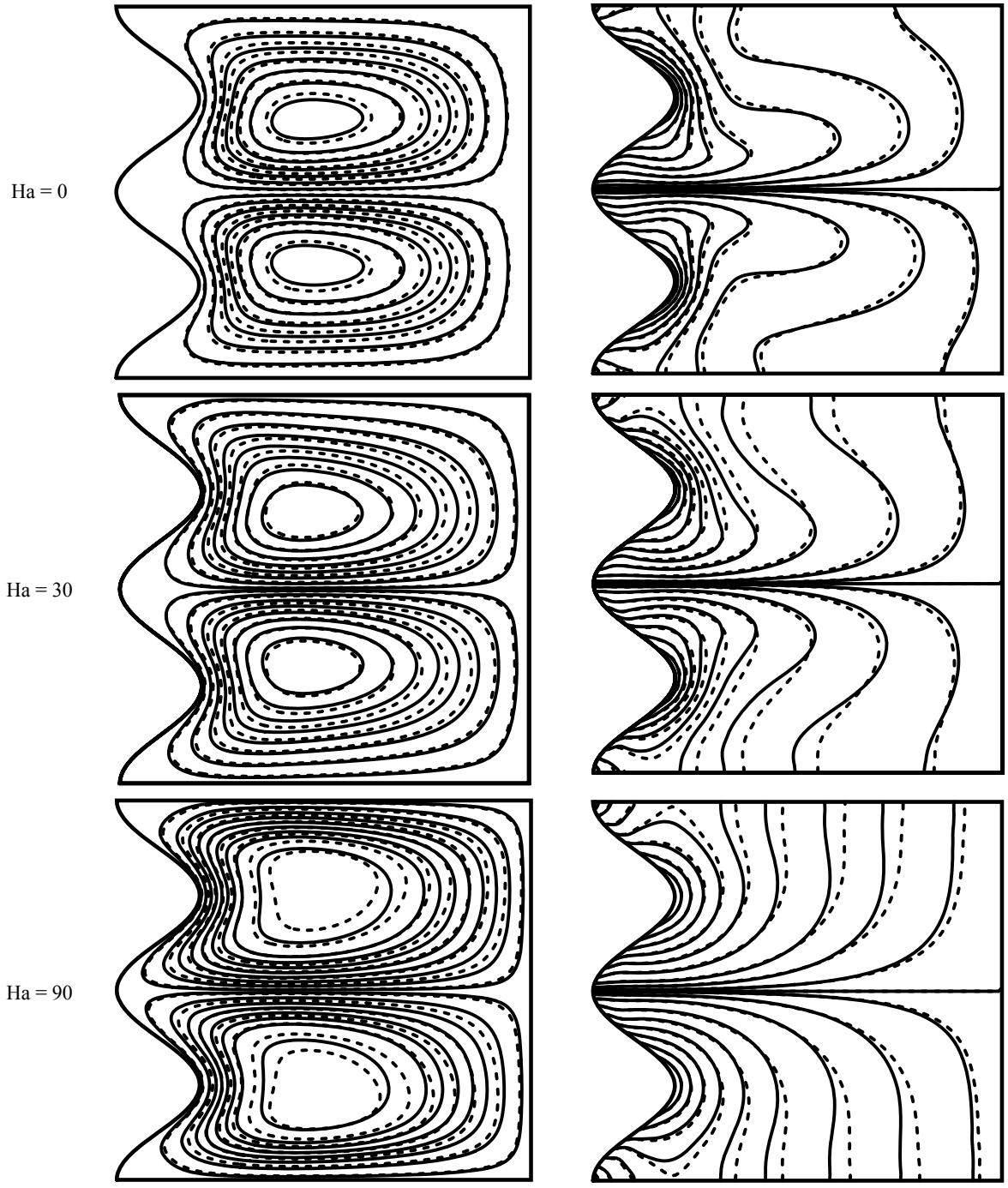

Fig. 12. Comparison of streamlines (left) and isotherms (right) for pure water (solid line) and nanofluid with $\varphi = 0.04$ (dashed line) at $Ra = 10^5$ and $\Phi = 0$

Figure 13 illustrates comparison of mean Nusselt number and normalized mean Nusselt number (Nu*) as a function of Hartman number for various Rayleigh numbers. It exhibits that the mean Nusselt number increases steadily and linearly by increasing volume fraction of nanoparticles for all cases of Rayleigh and Hartman numbers. However, the effect of volume fraction of nanoparticles on heat transfer rate is dissimilar at different Rayleigh numbers.

Thus, the normalized mean Nusselt number is the best parameter for observing of the effect of increasing volume fraction of nanoparticles to the pure fluid. At $Ra = 10^3$, the augmentation of Hartmann number plummets the effect of nanoparticles on heat transfer.

At Ra =10^4, the enhancement of Hartmann number exert a positive impact in the improvement of nanoparticles effect on heat transfer. At Ra = 10^5, the most improvement in heat transfer with the addition of the nanoparticles occurred in Ha = 90 while the least improvement was acquired in Ha=30.

Phase deviation of sinusoidal boundary condition

For this section of the study, the effect of phase deviation of sinusoidal boundary condition on flow and heat transfer has been analyzed for different Rayleigh numbers while the other parameters are kept constant at Ha = 30 and φ = 0.04.

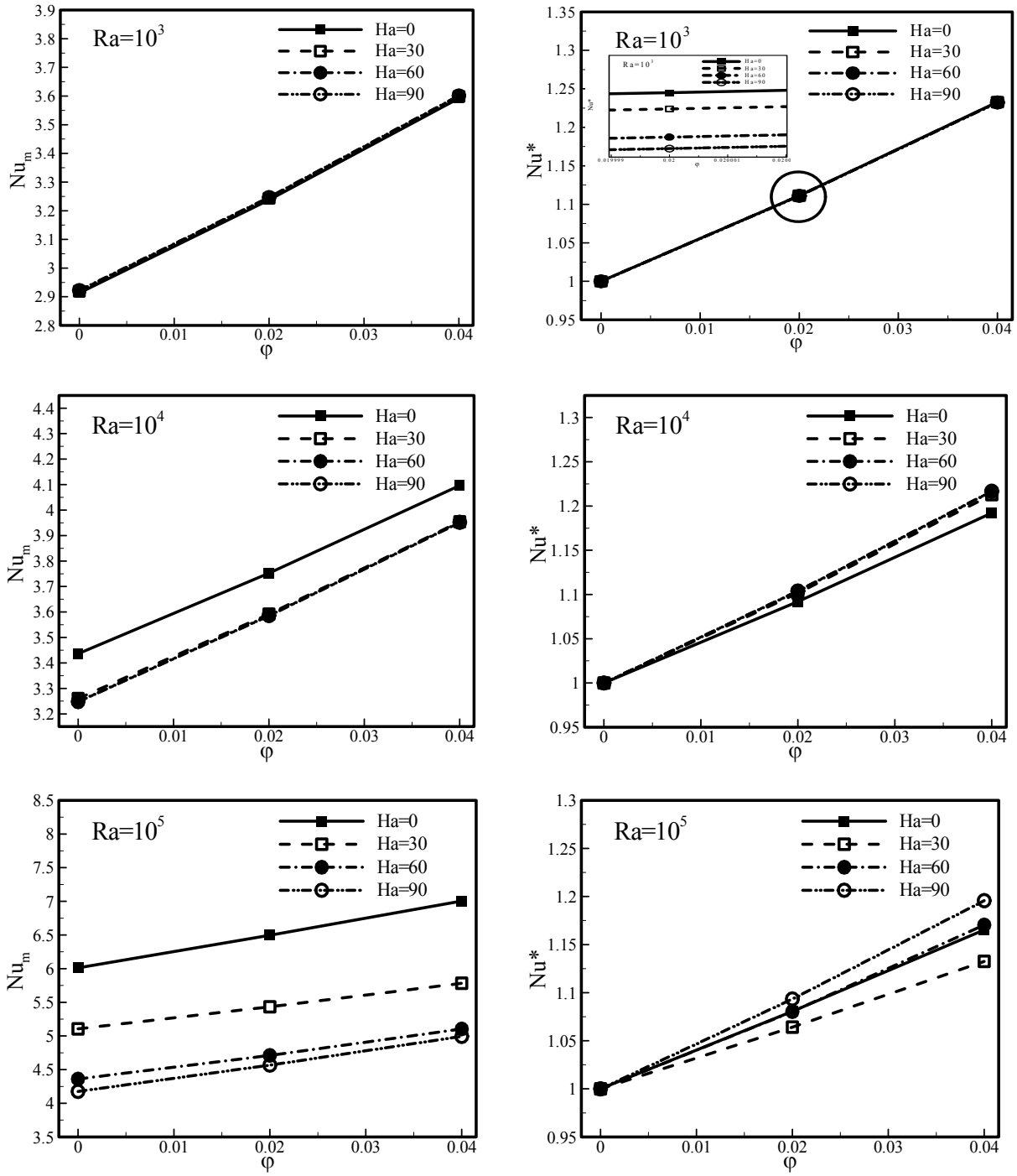

Fig. 13. Variation of mean Nusselt number (left) and normalized mean Nusselt number (right) at different volume fractions, Rayleigh numbers and Hartmann numbers (Φ = 0)

Figures 14 and 15 illustrate the effect of phase deviation ($\Phi = 0, \pi/2$ and π) for different values of the Rayleigh number ($Ra = 10^3$, 10^4 and 10^5) and $Ha = 30$ on flow and temperature distribution of nanofluid with $\varphi = 0.04$. For $\Phi = 0$, the left wall is heated from the bottom half and cooled.

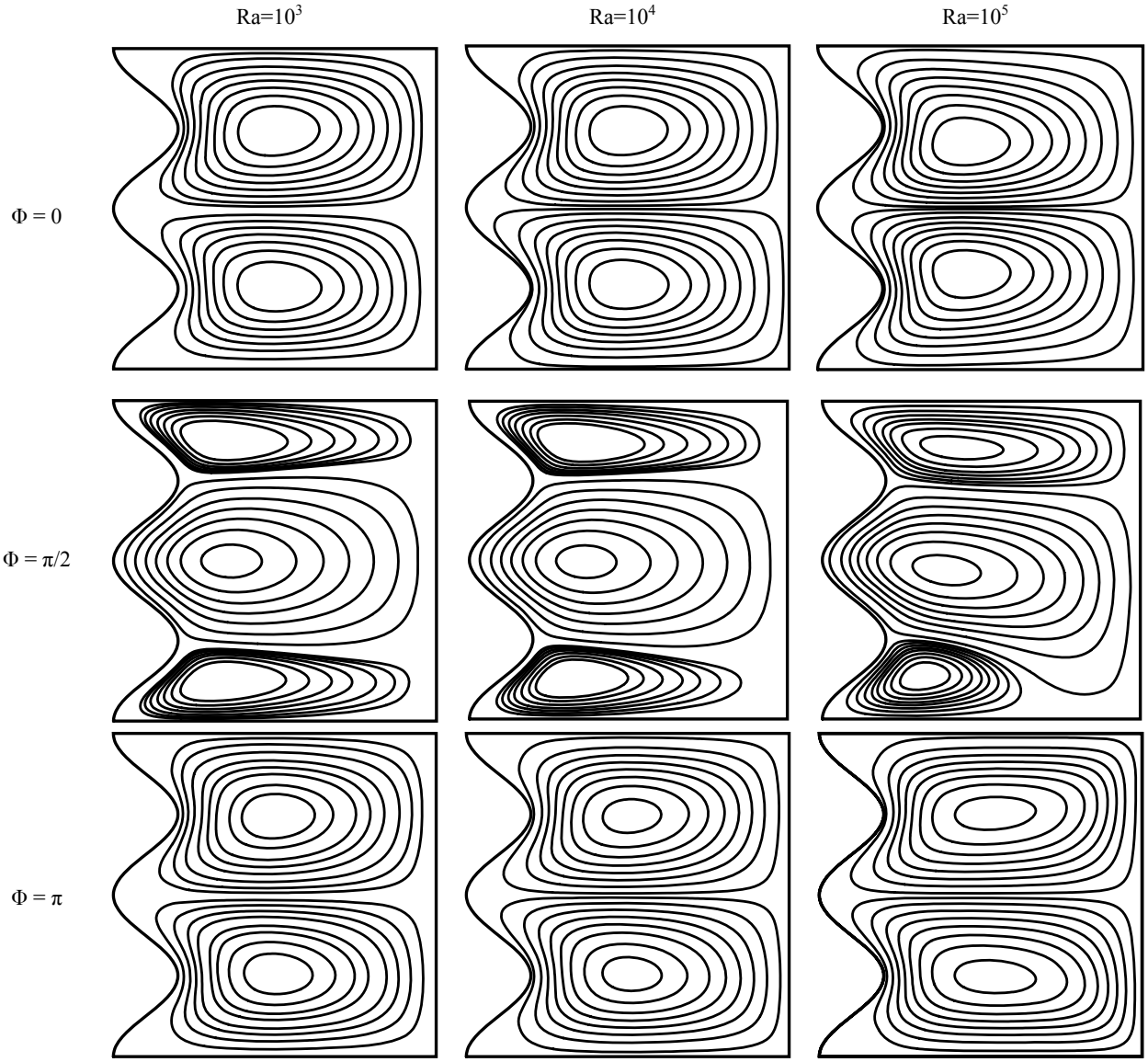

Fig. 14. Comparison of the streamlines contours for different Rayleigh numbers and phase deviations (Ha = 30 and φ = 0.04)

The streamlines show two circulation cells rotating in opposite directions, a clockwise circulation cell in bottom part and other in the top part of the cavity. The flow fields and temperature distribution is changed drastically with the growth of phase deviation from 0 to $\Phi = \pi/2$. The isotherms consisted a central heat sink and two heat sources at the top and bottom part of the left vertical wall. Therefore, the corresponding streamlines reflect a three-cellular structure with one large central cell and two smaller cells of identical sizes located on both sides.

Also, increasing of the Rayleigh number causes an intensification and increase in sizes of both clockwise and anti-clockwise vortexes located in the upper part of the cavity, but an attenuation and decrease in sizes of lower left-corner cell.

Furthermore, the symmetrical structures for isotherms is broken at $Ra = 10^5$ only for $\Phi = \pi/2$. As the phase deviation increases up to $\Phi = \pi$, symmetrical structures for the flow

and thermal fields are observed, but the heat sink/or source changed their position to opposite sides with respect to Φ = 0. Figure 16 illustrates variation of the local Nusselt number along hot wavy wall surface for different phase deviations at two Rayleigh numbers (Ra = 10^3 and Ra = 10^5).

This figure demonstrates that the local Nusselt number profiles along the left wavy wall is significantly affected due to changing the phase deviation. This result can be explained by noting that the heat source/ or sink position along the left wavy wall is associated with the values of phase deviation. At Φ = π/2 and Ra = 10^3, the heat conduction regime is dominant and isotherms are parallel to each other in vicinity of heat source/ or sink.

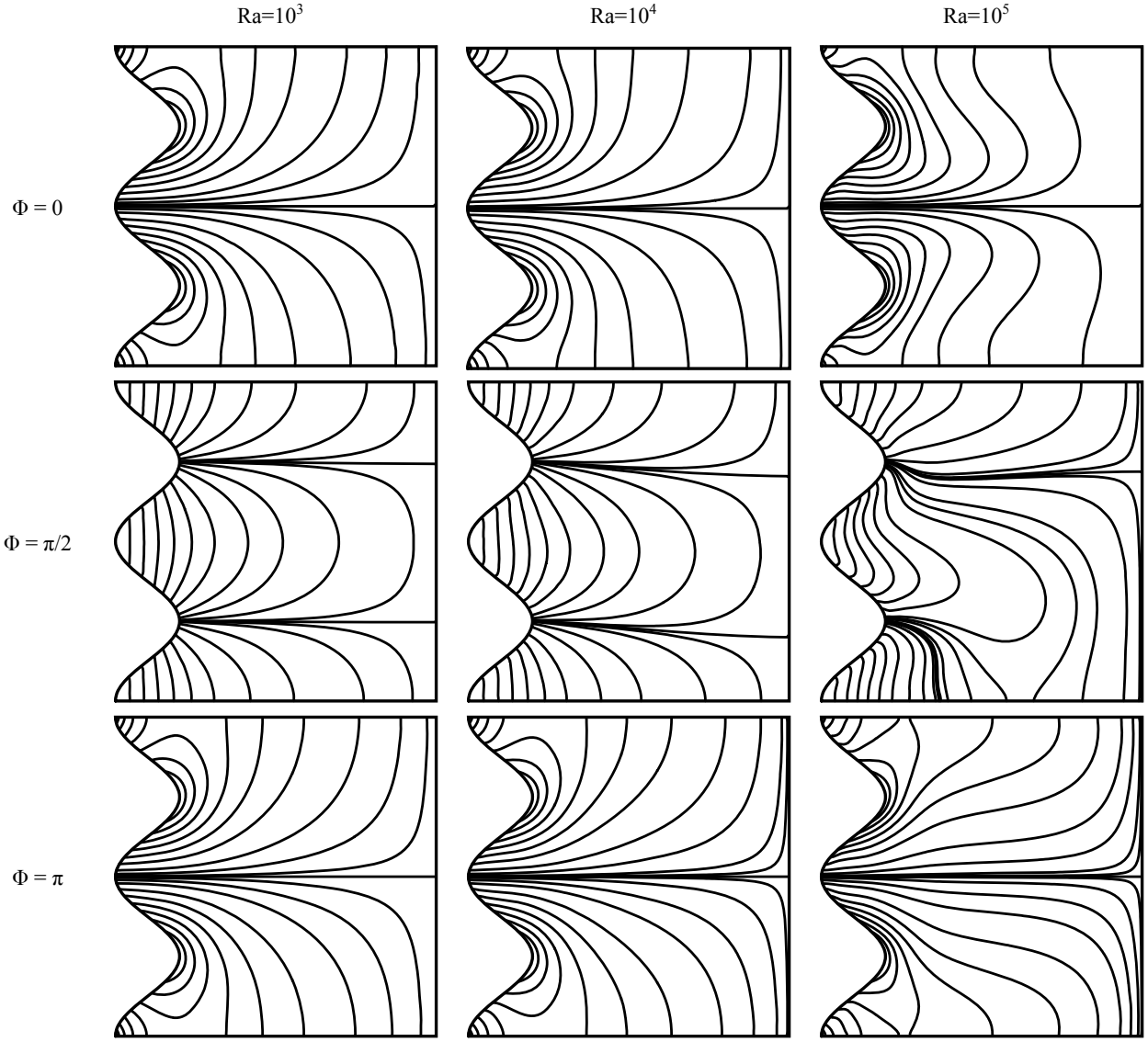

Fig. 15. Comparison of the isotherms contours for different Rayleigh numbers and phase deviations (Ha = 30 and φ = 0.04)

Thus, the local Nusselt number is approximately constant in these particular regions. At this phase deviation, as the Rayleigh number was increased beyond 10^4, isotherms reflect more distortion and a different local Nusselt number profile with Ra = 10^3. It is interesting to note that the variations with positive and negative values appeared in the local Nusselt numbers are corresponding to heating and cooling, respectively. This means that for positive local Nusselt number, the nanofluid receives heat energy from hot wavy wall and, in contrast, for negative values the wavy wall mainly gains heat energy from nanofluid.

Figure 17 depicts variations of dimensionless mean Nusselt number with volume fractions as a function of phase deviations of boundary conditions. This figure shows that dimensionless average Nusselt number increases by increasing volume fraction of nanoparticles for all phase deviations and Rayleigh numbers.

In general, for all Rayleigh numbers and volume fractions, the heat transfer augments with the growth of phase deviations from $\Phi = 0$ to $\pi/2$.

At Ra $=10^3$ and 10^4, the effect of phase deviation on heat transfer is erratic as the most heat transfer obtained in $\Phi = \pi/2$. At Ra $= 10^5$, the increment of the phase deviation has a positive role in the improvement of nanoparticles effect on heat transfer and least heat transfer was acquired at $\Phi = 0$, that is, in the absence of phase deviation.

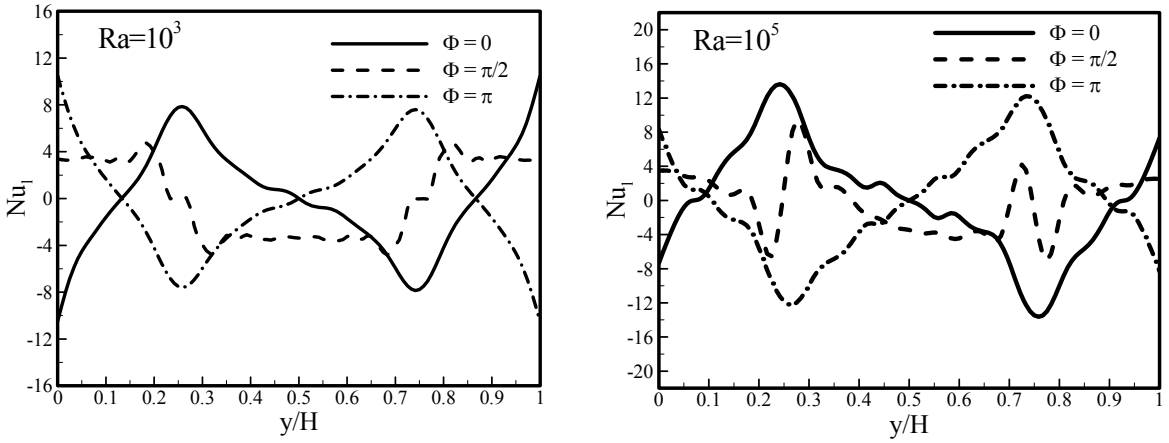

Fig. 16. Variation of local Nusselt number along hot wavy-wall surface for different phase deviations (Ha = 30 and φ = 0.04)

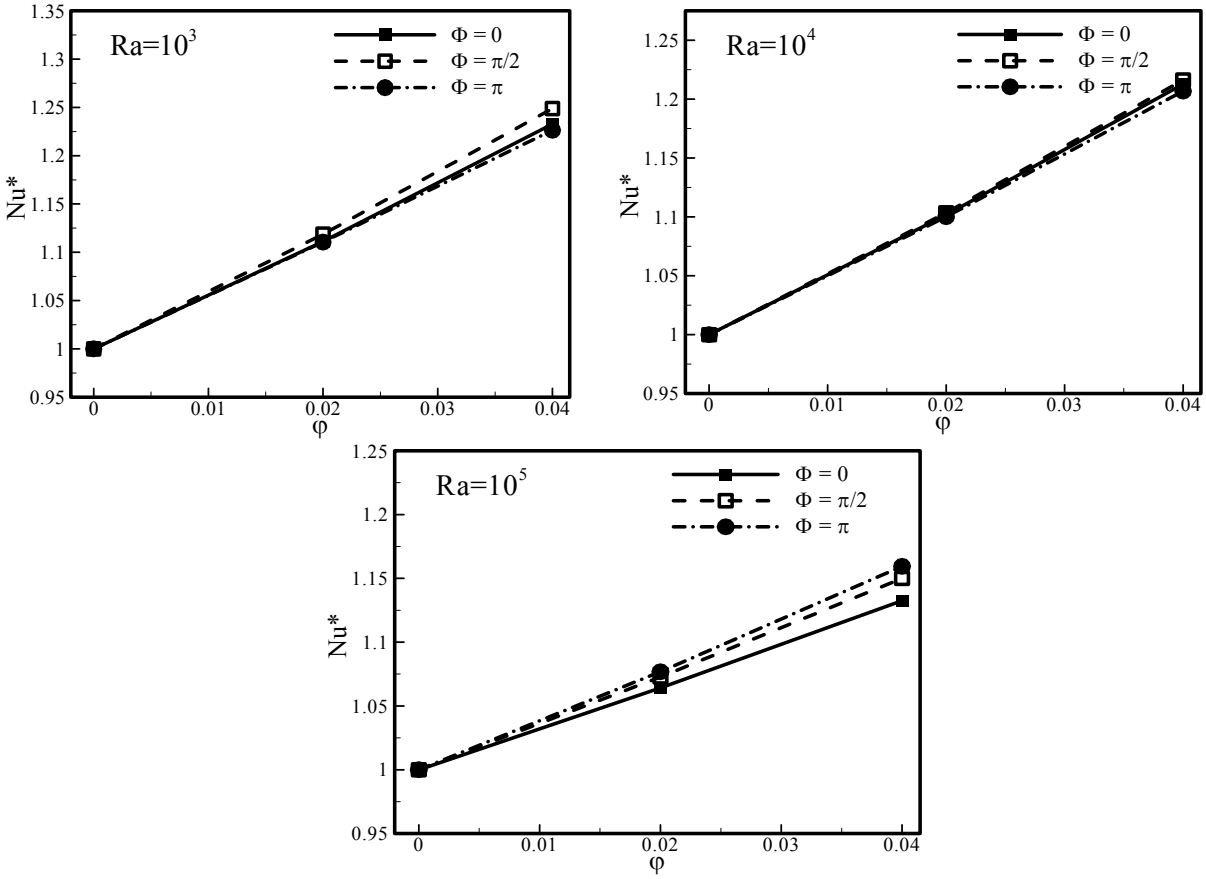

Fig. 17. Variation of normalized mean Nusselt number, at different volume fractions and Rayleigh numbers (Ha = 30)

CONCLUSION

In the present study, lattice Boltzmann method was employed to study laminar natural convection heat transfer of CuO-water nanofluid within a wavy-walled cavity with a sinusoidal thermal boundary condition and subjected to a uniform magnetic field.

The effect of Rayleigh number ($Ra = 10^3$ to 10^5), Hartmann number (Ha = 0 to 90), nanoparticle volume fraction ($0 < \varphi < 0.04$) and phase deviation ($\Phi = 0, \pi/2$ and π)

on the fluid flow and heat transfer, as well as mean Nusselt numbers were investigated.

This numerical analysis was performed for various values of above mentioned parameters with results summarized as follows:

a) Validation of present numerical results with available numerical results demonstrate that the LBM has the ability to predict the correct behavior for different applicable problems.

b) The intersection of isotherm line with the wavy wall due to non-uniform temperature distribution causes formation of cells on wavy wall. The numbers of these cells depend on the number of heat source or sink.

c) As the Hartmann number increases, the strength of the circulation structure within the cavity reduces as maximum decreasing rate of $|\psi_{max}|$ is about 7.8% that occurs for $Ra = 10^5$.

d) The effect of Hartmann number on heat transfer is opposite to the behavior registered of Rayleigh number except for $Ra = 10^3$. For Ha = 90, the decrement in normalized mean Nusselt number for $Ra = 10^4$ is about 4% whereas the decrease is around 29% for $Ra = 10^5$.

e) The mean Nusselt number increases steadily and linearly by increasing volume fraction of nanoparticles for all cases of Rayleigh and Hartman numbers. At $Ra = 10^5$, the most improvement in heat transfer with the addition of the nanoparticles occurred in Ha = 90 while the least improvement was acquired in Ha=30.

f) In general, for all Rayleigh numbers and volume fractions, the heat transfer augments with the growth of phase deviations from $\Phi = 0$ to $\pi/2$, for Ha = 30.
At $Ra = 10^3$ and 10^4, the effect of phase deviation on heat transfer is erratic as the most heat transfer obtained in $\Phi = \pi/2$.

REFERENCES

[1] de Vahl Davis G.Natural convection of air in a square cavity: a bench mark numerical solution. International Journal for numerical methods in fluids. 1983 May 1;3(3):249-64.

[2] Barakos G, Mitsoulis E, Assimacopoulos D. Natural convection flow in a square cavity revisited: laminar and turbulent models with wall functions. International Journal for Numerical Methods in Fluids. 1994 Apr 15;18(7):695-719.

[3] Fusegi T, Hyun JM, Kuwahara K, Farouk B.A numerical study of three-dimensional natural convection in a differentially heated cubical enclosure. International Journal of Heat and Mass Transfer. 1991 Jun 1;34(6):1543-57.

[4] Chol SU. Enhancing thermal conductivity of fluids with nanoparticles. ASME-Publications-Fed. 1995 Nov 12;231:99-106.

[5] Kim J, Kang YT, Choi CK. Analysis of convective instability and heat transfer characteristics of nanofluids. Physics of fluids. 2004 Jul;16(7):2395-401.

[6] Putra N, Roetzel W, Das SK. Natural convection of nano-fluids. Heat and Mass Transfer. 2003 Sep 1;39(8-9):775-84.

[7] Khanafer K,Vafai K, Lightstone M.Buoyancy-driven heat transfer enhancement in a two-dimensional enclosure utilizing nanofluids. International journal of heat and mass transfer. 2003 Sep 30;46(19):3639-53.

[8] Rudraiah N, Barron RM, Venkatachalappa M, Subbaraya CK. Effect of a magnetic field on free convection in a rectangular enclosure. International Journal of Engineering Science. 1995 Jun 1;33(8):1075-84.

[9] Kahveci K, Öztuna S. MHD natural convection flow and heat transfer in a laterally heated partitioned enclosure. European Journal of Mechanics-B/Fluids. 2009 Dec 31;28(6):744-52.

[10] Sathiyamoorthy M, Chamkha A. Effect of magnetic field on natural convection flow in a liquid gallium filled square cavity for linearly heated side wall (s). International Journal of Thermal Sciences. 2010 Sep 30;49(9):1856-65.

[11] Saha LK, Hossain MA, Gorla RS. Effect of Hall current on the MHD laminar natural convection flow from a vertical permeable flat plate with uniform surface temperature. International journal of thermal sciences. 2007 Aug 1;46(8):790-801.

[12] Oztop HF, Oztop M, Varol Y. Numerical simulation of magnetohydrodynamic buoyancy-induced flow in a non-isothermally heated square enclosure. Communications in Nonlinear Science and Numerical Simulation. 2009 Mar 31;14(3):770-8.

[13] Succi S. The lattice Boltzmann equation: for fluid dynamics and beyond. Oxford university press; 2001 Jun 28.

[14] Aidun CK, Clausen JR. Lattice- Boltzmann method for complex flows. Annual review of fluid mechanics. 2010;42:439-72.

[15] Gao D, Chen Z. Lattice Boltzmann simulation of natural convection dominated melting in a rectangular cavity filled with porous media. International Journal of Thermal Sciences. 2011 Apr 30;50(4):493-501.

[16] Filippova O, Hänel D. Boundary-fitting and local grid refinement for lattice-BGK models. International Journal of Modern Physics C. 1998 Dec;9(08):1271-9.

[17] Mei R, Luo LS, Shyy W.An accurate curved boundary treatment in the lattice Boltzmann method. Journal of computational physics. 1999 Nov 1;155(2):307-30.

[18] Guo Z, Zheng C, Shi B. Discrete lattice effects on the forcing term in the lattice Boltzmann method. Physical Review E. 2002 Apr 10;65(4):046308.

[19] Ghasemi B, Aminossadati S , Raisi A. Magnetic field effect on natural convection in a nanofluid-filled square enclosure. International Journal of Thermal Sciences. 2011 Sep 30;50(9):1748-56.

[20] Kefayati GR. Effect of a magnetic field on natural convection in an open cavity subjugated to water/alumina nanofluid using Lattice Boltzmann method. International Communications in Heat and Mass Transfer. 2013 Jan 31;40:67-77.

[21] Kefayati GR. Lattice Boltzmann simulation of MHD natural convection in a nanofluid-filled cavity with sinusoidal temperature distribution. Powder technology. 2013 Jul 31;243:171-83.

[22] Mliki B, Abbassi MA, Omri A, Zeghmati B. Augmentation of natural convective heat transfer in linearly heated cavity by utilizing nanofluids in the presence of magnetic field and uniform heat generation/absorption. Powder Technology. 2015 Nov 30;284:312-25.

[23] Sheikholeslami M, Gorji-Bandpy M, Ganji D. Investigation of Nanofluid Flow and Heat Transfer in Presence of Magnetic Field Using KKL Model. Arabian Journal for Science & Engineering (Springer Science & Business Media BV). 2014 Jun 1;39(6).

[24] Sheremet MA, Pop I, Roşca NC. Magnetic field effect on the unsteady natural convection in a wavy-walled cavity filled with a nanofluid: Buongiorno's mathematical model. Journal of the Taiwan Institute of Chemical Engineers. 2016 Apr 30;61:211-22.

[25] Sabeur-Bendehina A, Imine O, Adjlout L. Laminar free convection in undulated cavity with non-uniform boundary conditions. Comptes Rendus Mécanique. 2011 Jan 1;339(1):42-57.

[26] A. Shahriari: Numerical simulation of free convection heat transfer of nanofluid in a wavy-wall cavity with sinusoidal temperature distribution, using lattice Boltzmann method, Modares Mechanical Engineering 16 (2016) 143-154.

[27] Xuan Y, Roetzel W. Conceptions for heat transfer correlation of nanofluids. International Journal of heat and Mass transfer. 2000 Oct 1;43(19):3701-7.

[28] Brinkman HC. The viscosity of concentrated suspensions and solutions. The Journal of Chemical Physics. 1952 Apr;20(4):571-.

[29] Hamilton RL, Crosser OK. Thermal conductivity of heterogeneous two-component systems. Industrial & Engineering chemistry fundamentals. 1962 Aug;1(3):187-91.

[30] Kao PH, Yang RJ. Simulating oscillatory flows in Rayleigh–Benard convection using the lattice Boltzmann method. International Journal of Heat and Mass Transfer. 2007 Aug 31;50(17):3315-28.

[31] Chen S, Doolen GD. Lattice Boltzmann method for fluid flows. Annual review of fluid mechanics. 1998 Jan;30(1):329-64.

[32] Sheikholeslami M, Gorji-Bandpy M, Vajravelu K. Lattice Boltzmann simulation of magnetohydrodynamic natural convection heat transfer of Al_2O_3–water nanofluid in a horizontal cylindrical enclosure with an inner triangular cylinder. International Journal of Heat and Mass Transfer. 2015 Jan 31;80:16-25.

[33] Tiwari RK, Das MK. Heat transfer augmentation in a two-sided lid-driven differentially heated square cavity utilizing nanofluids. International Journal of Heat and Mass Transfer. 2007 May 31;50(9):2002-18.

[34] Lin KC, Violi A. Natural convection heat transfer of nanofluids in a vertical cavity: Effects of non-uniform particle diameter and temperature on thermal conductivity. International Journal of Heat and Fluid Flow. 2010 Apr 30;31(2):236-45.

[35] Krane RJ, Jessee J. Some detailed field measurements for a natural convection flow in a vertical square enclosure. In1st ASME-JSME thermal engineering joint conference 1983 Mar 20 (Vol. 1, pp. 323-329). ASME New York.

[36] Oztop HF, Abu-Nada E. Numerical study of natural convection in partially heated rectangular enclosures filled with nanofluids. International journal of heat and fluid flow. 2008 Oct 31;29(5):1326-36.

[37] Cho CC, Chen CL. Natural convection heat transfer performance in complex-wavy-wall enclosed cavity filled with nanofluid. International Journal of Thermal Sciences. 2012 Oct 31;60:255-63.

[38] Kefayati GR. Lattice Boltzmann simulation of natural convection in nanofluid-filled 2D long enclosures at presence of magnetic field. Theoretical and Computational Fluid Dynamics. 2013 Nov 1:1-9.

[39] Ahrar AJ, Djavareshkian MH. Lattice Boltzmann simulation of a Cu-water nanofluid filled cavity in order to investigate the influence of volume fraction and magnetic field specifications on flow and heat transfer. Journal of Molecular Liquids. 2016 Mar 31;215:328-38.